Update of the EPTN atlas for CT- and MR-based contouring in Neuro-Oncology

Eekers, D.B.P.; Perri, D. di; Roelofs, E.; Postma, A.; Dijkstra, J.; Ajithkumar, T.; ... ; Troost, E.G.C.

Radiotherapy and Oncology 160 (2021) 259–265

Contents lists available at ScienceDirect

Radiotherapy and Oncology

journal homepage: www.thegreenjournal.com

Original Article

Update of the EPTN atlas for CT- and MR-based contouring in Neuro-Oncology

Daniëlle B.P. Eekers [a,1,*], Dario Di Perri [b,1], Erik Roelofs [a,1], Alida Postma [c,1], Jeanette Dijkstra [d,1], Thankamma Ajithkumar [e,1,2], Claire Alapetite [f,1,2], Malin Blomstrand [g,1], Neil G Burnet [h,1], Valentin Calugaru [i,j,1], Inge Compter [a,1], Ida E.M. Coremans [k,l,1], Semi Harrabi [m,1], Alberto Iannalfi [n,1], Yvonne L.B. Klaver [k,l,p,1], Maarten Lambrecht [o,1], Alejandra Méndez Romero [l,p,1], Frank Paulsen [q,1], Beate Timmermann [r,s,t,1,2], Pavel Vitek [u,1], Hiske L van der Weide [v,1], Gillian A Whitfield [w,x,1], Petra Witt Nyström [y,1], Jaap Zindler [l,z,1], Dirk de Ruysscher [a,1], Johannes Langendijk [v,1], Damien C Weber [aa,1], Esther G.C. Troost [ab,ac,ad,ae,af,ag,ah,ai,1]

[a] Department of Radiation Oncology (Maastro), GROW School for Oncology, Maastricht University Medical Centre+, The Netherlands; [b] Department of Radiation Oncology, Cliniques universitaires Saint-Luc, Brussels, Belgium; [c] Department of Radiology and Nuclear Medicine MUMC+, Maastricht, The Netherlands; [d] Department of Medical Psychology MUMC+, Maastricht, The Netherlands; [e] Department of Oncology, Cambridge University Hospitals NHS Foundation Trust, United Kingdom; [f] Institut Curie, Radiation Oncology Department, Paris & Proton Center, Orsay, France; [g] Department of Oncology, Sahlgrenska University Hospital Gothenburg, Sweden; [h] The Christie NHS Foundation Trust, Manchester, United Kingdom; [i] Institute Curie, Paris, France; [j] Institute Curie, Centre de Protonthérapie d'Orsay, Orsay, France; [k] Leiden University Medical Centre, Department of Radiotherapy, Leiden; [l] HollandPTC, Delft, The Netherlands; [m] Department of Radiotherapy, Heidelberg, Germany; [n] Clinical Department, Radiotherapy Unit, National Center for Oncological Hadrontherapy (CNAO), Pavia, Italy; [o] Department of Radiotherapy-Oncology, Leuven Kanker Instituut, UZ Gasthuisberg, Belgium; [p] Department of Radiotherapy, Erasmus MC Cancer Institute, Erasmus University Medical Centre, Rotterdam, The Netherlands; [q] Department of Radiation Oncology, Eberhard-Karls-Universität Tübingen; [r] Clinic for Particle Therapy, University Hospital Essen, West German Cancer Center (WTZ); [s] West German Proton Therapy Center Essen (WPE); [t] German Cancer Consortium (DKTK), partnersite Essen, Essen, Germany; [u] Proton Therapy Center Czech, Prague, Czech Republic; [v] Department of Radiation Oncology, University Medical Center Groningen, University of Groningen, The Netherlands; [w] The University of Manchester, Manchester Academic Health Science Centre, The Christie NHS Foundation Trust, United Kingdom; [x] The Children's Brain Tumour Research Network, University of Manchester, Royal Manchester Children's Hospital, United Kingdom; [y] Danish Centre for Particle Therapy, Aarhus, Denmark; [z] Haaglanden Medisch Centrum, Department of Radiotherapy, Leidschendam, The Netherlands; [aa] Paul Scherrer Institut, Center for Proton Therapy, Villigen-PSI, Switzerland; [ab] Department of Radiotherapy and Radiation Oncology, Faculty of Medicine and University Hospital Carl Gustav Carus, Technische Universität Dresden, Dresden; [ac] Helmholtz-Zentrum Dresden-Rossendorf, Institute of Radiooncology - OncoRay, Dresden; [ad] OncoRay – National Center for Radiation Research in Oncology, Faculty of Medicine and University Hospital Carl Gustav Carus, Technische Universität Dresden, Helmholtz-Zentrum Dresden - Rossendorf Dresden; [ae] German Cancer Consortium (DKTK), partnersite Dresden and German Cancer Research Center (DKFZ); [af] National Center for Tumor Diseases (NCT), Partner Site Dresden; [ag] German Cancer Research Center (DKFZ), Heidelberg; [ah] Faculty of Medicine and University Hospital Carl Gustav Carus, Technische Universität Dresden, Dresde; and [ai] Helmholtz Association / Helmholtz-Zentrum Dresden - Rossendorf (HZDR)., Germany

ARTICLE INFO

Article history:
Received 26 February 2021
Received in revised form 4 May 2021
Accepted 12 May 2021
Available online 18 May 2021

Keywords:
Atlas for neuro-oncology
Brain
Organs at risk
Particle therapy
Radiotherapy
European Particle Therapy Network

ABSTRACT

Background and purpose: To update the digital online atlas for organs at risk (OARs) delineation in neuro-oncology based on high-quality computed tomography (CT) and magnetic resonance (MR) imaging with new OARs.

Materials and methods: In this planned update of the neurological contouring atlas published in 2018, ten new clinically relevant OARs were included, after thorough discussion between experienced neuro-radiation oncologists (RTOs) representing 30 European radiotherapy-oncology institutes. Inclusion was based on daily practice and research requirements. Consensus was reached for the delineation after critical review. Contouring was performed on registered CT with intravenous (IV) contrast (soft tissue & bone window setting) and 3 Tesla (T) MRI (T1 with gadolinium & T2 FLAIR) images of one patient (1 mm slices). For illustration purposes, delineation on a 7 T MRI without IV contrast from a healthy volunteer was added. OARs were delineated by three experienced RTOs and a neuroradiologist based on the relevant literature.

Results: The presented update of the neurological contouring atlas was reviewed and approved by 28 experts in the field. The atlas is available online and includes in total 25 OARs relevant to neuro-

* Corresponding author at: MAASTRO Clinic, Doctor Tanslaan 12, 6229 ET Maastricht, The Netherlands.
E-mail address: danielle.eekers@maastro.nl (D.B.P. Eekers).
[1] On behalf of the taskforce "European Particle Therapy Network" of ESTRO.
[2] On behalf of SIOPE-BTG Radiotherapy Group.

https://doi.org/10.1016/j.radonc.2021.05.013

oncology, contoured on CT and MRI T1 and FLAIR (3 T & 7 T). Three-dimensional (3D) rendered films are also available online.
Conclusion: In order to further decrease inter- and intra-observer OAR delineation variability in the field of neuro-oncology, we propose the use of this contouring atlas in photon and particle therapy, in clinical practice and in the research setting. The updated atlas is freely available on www.cancerdata.org.
 Radiotherapy and Oncology 160 (2023) 259–265

In 2018, the European Particle Therapy Network (EPTN) presented a consensus-based contouring atlas for CT- and MR-based contouring in Neuro-Oncology [1,2]. This atlas is available online and is now being used internationally by radiation oncologists (RTOs) and radiation therapy technologists (RTTs) in daily practice, as well as for research purposes [3–6]. Since this time, the search for organs at risk (OARs) associated with toxicity has continued [7,8]. Also new potential toxicities have been described, e.g. MR changes observed in the periventricular space after particle therapy [9–12]. As a result, there is a need for an update of the atlas, with the addition of potentially clinically relevant OARs. In this context, the members of the EPTN taskforce joined efforts to create an updated atlas available online [13].

Selection of OARs

All 15 OARs presented in the atlas published in 2018 were contoured on a new patient high quality imaging study set, now also including a 3 Tesla (T) FLAIR sequence and 7 T MRI. OARs previously included are in alphabetical order: brain, brainstem (midbrain, pons, medulla oblongata), chiasm, cerebellum (anterior & posterior), cochlea, cornea, hippocampus (anterior & posterior), hypothalamus, lens, lacrimal gland, optic nerve, pituitary, skin, and vestibular and semicircular canals [1,2].

In order to further facilitate future research on cognitive functioning and radiological changes after irradiation of the brain, potentially clinically relevant OARs were further added: amygdala, caudate nucleus, corpus callosum, fornix, optic tract, orbitofrontal cortex, periventricular space (PVS), pineal gland, and thalamus. With increasing positioning accuracy up to 1 mm, the need for identifying the location of the macula when irradiating in proximity of the optical system was deemed necessary and added to the atlas.

Typical head and neck OARs (e.g. salivary glands), which are described in the head and neck atlas published by Brouwer et al. [14], were not included in the present atlas.

CT and MR acquisition

Acquisition details are described in our previous publication [2]. Briefly, a CT with iodine contrast and a 3 T MRI with gadolinium (1 mm slice thickness) were acquired in an adult patient with small brain metastases in supine position using a thermoplastic immobilization mask. Concerning the MRI scan, a post-gadolinium T1 sequence (T1Gd) as well as a T2 FLAIR sequence were acquired. The CT and MR scans were aligned using rigid registration (Eclipse™ VII.0, software, Varian, Palo Alto, CA and Raystation®, V10A, Raysearch Laboratories, Stockholm). In addition, a 7 T MRI scan (MP2RAGE sequence, 0.7 mm slice thickness) was acquired on a healthy volunteer [15].

Uniform nomenclature

The nomenclature introduced by Santanam et al. [16] was used, e.g. thalamus: "Thalamus_L", "Thalamus_R", "Thalami". For structures not visible on imaging a reconstruction based on visual anatomy was made adding "rc" to the OAR name, e.g. left fovea: "Fovea_L_rc".

Delineation

Twenty-five OARs were delineated by three experienced RTOs (DE, DDP, and IC) and a neuroradiologist (AP): 15 previously described [1,2] and 10 added in the present update of the atlas. Delineation was performed using the high-resolution segment of the radiation treatment planning software (Eclipse™ VII.0, software, Varian, Palo Alto, CA and Raystation®, V10A, Raysearch Laboratories, Stockholm). Consensus was reached after multiple multidisciplinary meetings, resulting in a first draft of the atlas. This version was carefully reviewed by 28 experts from 30 radiotherapy-oncology institutes throughout Europe.

Three-dimensional description of the organs at risk

1. *Amygdala ('Amygdala_R" and "Amygdala_L")*

The amygdala, which is part of the limbic system, plays a key-role in emotional functioning. It is notably involved in the processing of information coming from the thalamus and from the sensory and association cortices [17].

Each amygdala should be contoured separately. Co-registration with T1-weighted MRI is required for delineation. The amygdala (Fig. 1) is an olive-shaped gray matter structure located in the anteromedial part of the temporal lobe and measuring 1–2 cm^3. It is bounded anteriorly and medially by the cortex of the temporal lobe and posteriorly and inferiorly by the temporal horn of the lateral ventricle and by the hippocampus. The amygdala is separated from the hippocampus by a thin layer of white matter known as the alveus. Laterally, the amygdala is bordered by the white fibres of the temporal lobe [18,19].

2. *Caudate nucleus ("CaudateNucleus_R" and "CaudateNucleus_L")*

Besides its classical role in motor control, the caudate nucleus (Figs. 1–3) also plays a role in cognitive and emotional processing [20]. The caudate nucleus is part of the basal ganglia, together with the putamen and the globus pallidus. The complex formed by the caudate nucleus and the putamen is also referred as *striatum* (or *neostriatum*) [18].

Each caudate nucleus should be contoured separately. Co-registration with T1-weighted MRI is required for delineation. The caudate nucleus is a curved, tadpole-shaped, structure composed of three parts: a large anterior head, a tapering body, and a thin tail, which wraps around the thalamus, following the curvature of the lateral ventricle. It is isointense to cortex on T1-imaging. The head of the caudate nucleus forms the lateral wall of the anterior horn of the lateral ventricle and meets the putamen anterolaterally, and the nucleus accumbens inferiorly. The body of the caudate nucleus lies lateral to the lateral ventricle, and medial to the internal capsule. The tail curves back anteriorly along the roof of the temporal horn of the lateral ventricle, and ends in the amygdala [18]. The last part of the tail can be difficult to identify on commonly acquired MRI scans (i.e. 1.5–3 T).

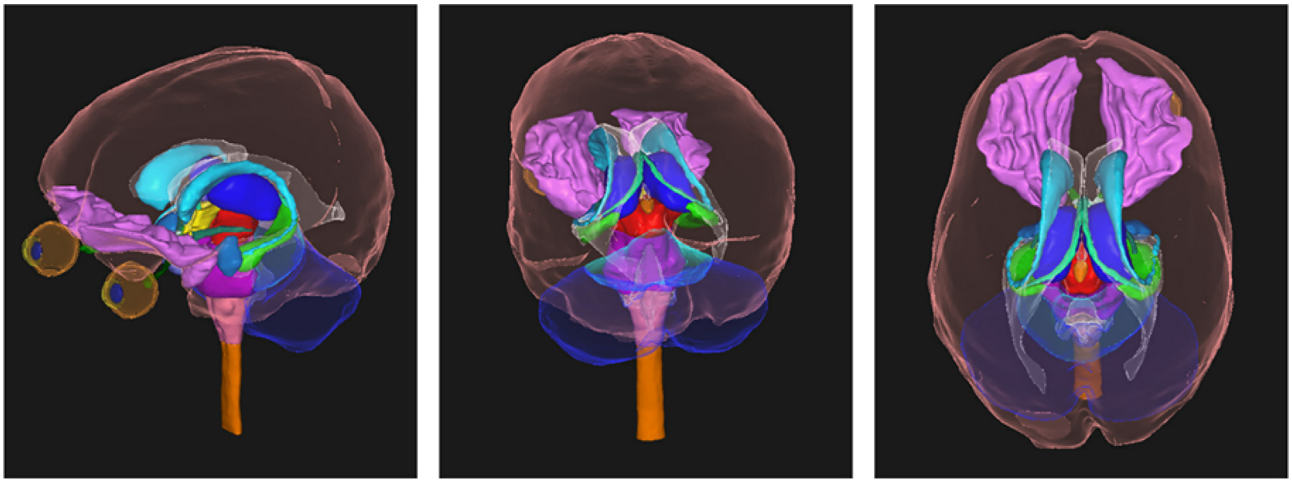

Fig. 1. Visualisation of the organs at risk in three-dimensional rendering. Colour legend (in alphabetical order): Amygdala: light blue; Brainstem [Midbrain: red, Pons: purple, Medulla oblongata: pink]; Caudate nucleus: cyan; Cerebellum [anterior: semi-transparent light blue, posterior: semi-transparent blue]; Cornea: semi-transparent yellow; Fornix: green; Hippocampus: spring green; Hypothalamus: yellow; Lens: blue; Orbitofrontal cortex: pink; Optic nerve: green; Optic tract: dark green; Pineal gland: orange; Retina: semi-transparent orange; Spinal cord: orange; Supratentorial brain: semi-transparent pink; Thalamus: blue; Ventricles: semi-transparent white.

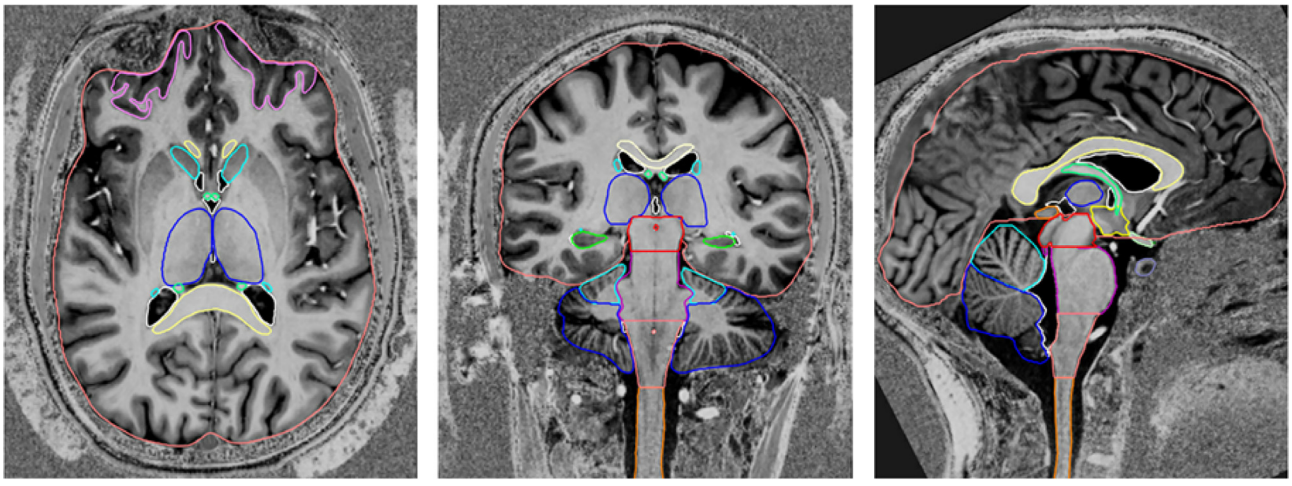

Fig. 2. Visualisation of the organs at risk on a 7 T MRI (MP2RAGE) scan (from left to right: axial, coronal, and sagittal planes). Colour legend (in alphabetical order): Brainstem [Midbrain: red, Pons: purple, Medulla oblongata: pink]; Caudate nucleus: cyan; Cerebellum [anterior: cyan, posterior: blue]; Corpus Callosum: pale yellow; Fornix: green; Hippocampus: green; Hypothalamus: yellow; Orbitofrontal cortex: pink; Optic chiasm: light green; Pineal gland: orange; Pituitary: lavender; Spinal cord: orange; Supratentorial brain: salmon; Thalamus: blue; Ventricles: white.

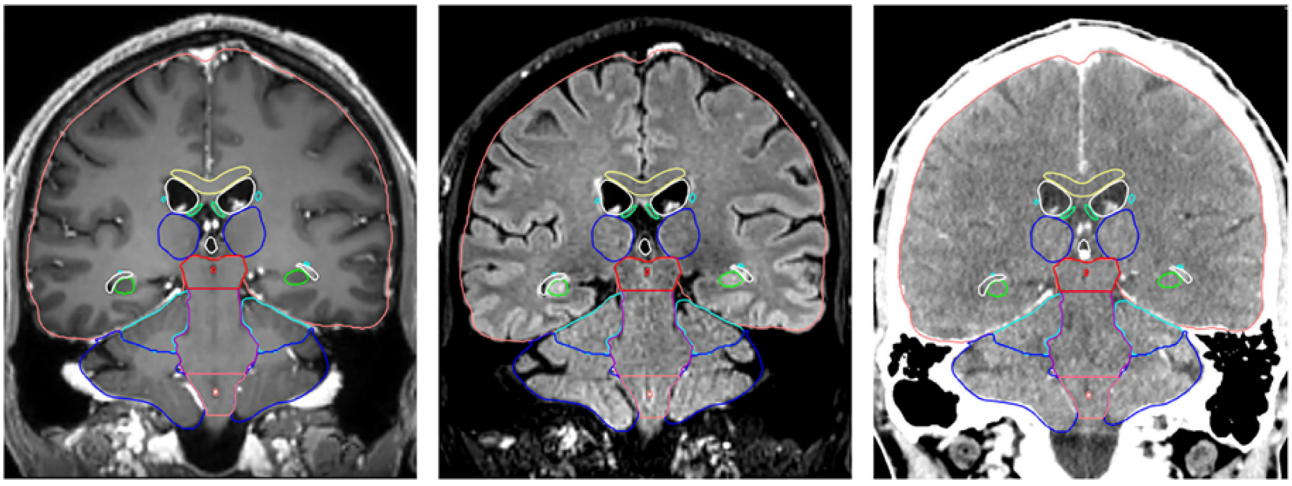

Fig. 3. Visualisation of the organs at risk in the coronal plane, from left to right: 3 T MRI T1Gd, 3 T MRI T2 FLAIR, and CT (brain window). Colour legend (in alphabetical order): Brainstem [Midbrain: red, Pons: purple, Medulla oblongata: pink]; Caudate nucleus: cyan; Cerebellum [anterior: cyan, posterior: blue]; Corpus Callosum: pale yellow; Fornix: green; Hippocampus: green; Supratentorial brain: salmon; Thalamus: blue; Ventricles: white.

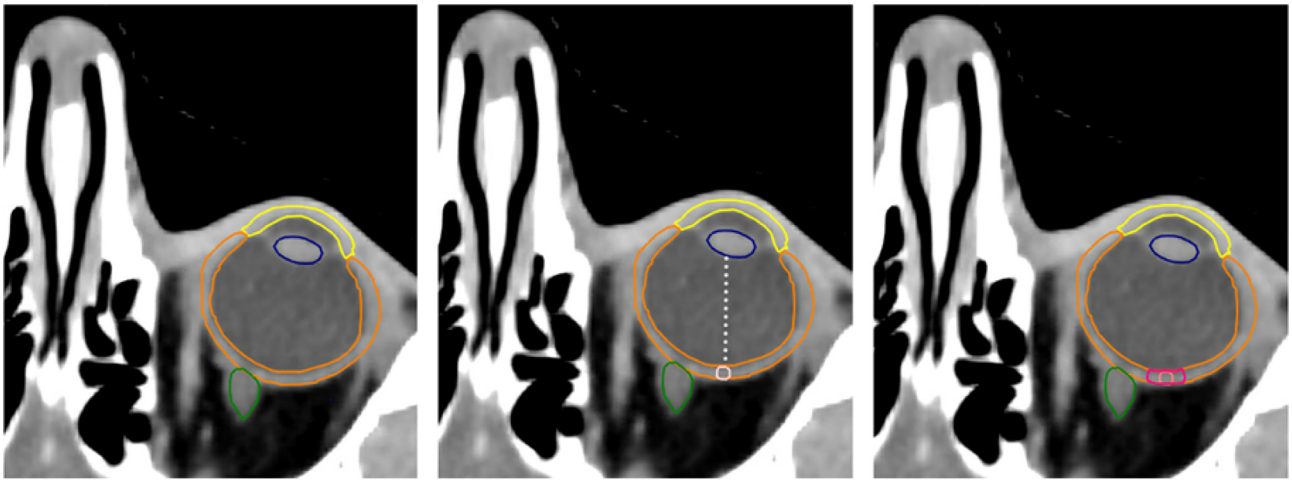

Fig. 4. Proposed delineation method for the fovea and the macula. Colour legend (in alphabetical order): Cornea: yellow; Fovea (*reconstructed*): pink; Lens: blue; Macula (*reconstructed*): purple red; Optic nerve: green; Retina: orange.

3. *Thalamus ("Thalamus_R" and "Thalamus_L")*

The thalamus (Figs. 1–3) is a relay station for most sensory information but also plays a role in cognition (e.g. learning, memory, and flexible adaptation) [21].

Each thalamus should be contoured separately. Co-registration with T1-weighted MRI is required for delineation. The thalami are egg-shaped grey-matter masses, about 4 cm long, which can be asymmetrical. Medially, they are bounded by the third ventricle, through which they are frequently connected (interthalamic adhesion). Laterally, they are bounded by the posterior limb of the internal capsule. The anterior border of the thalamus reaches the level of the interventricular foramen, while the posterior border abuts the atrium of the lateral ventricle. Superiorly, each thalamus forms part of the floor of the lateral ventricle. Inferiorly, the thalami are limited by the hypothalamus anteriorly and by the midbrain posteriorly [18,19].

4. *Macula ("Macula_R_rc" and "Macula_L_rc")*

Each macula should be contoured separately. The macula is the central region of the retina. It is an oval-shaped area measuring 5–6 mm in diameter and located approximately 4 mm temporal and 0.8 mm inferior to the centre of the head of the optic nerve. The fovea is approximately located at the centre of the macula and is the most sensitive part of the retina [22]. The macula cannot be distinguished from the rest of the retina on CT or MR imaging. For the purpose of macula avoidance, a surrogate region can nevertheless be delineated as follows (Fig. 4):

- select the slice going through the centre of the lens and the optic nerve
- using a 1 mm-brush contour the region of the retina which is located in line with the centre of the lens, it must be located at least 2-mm lateral to the optic nerve. This region is the reconstructed (rc) location of the fovea, and is named fovea_rc
- create an outer margin of 2 mm around fovea_rc
- erase the parts which are inside (vitreous body) and outside (fat) the eye, keeping only the retina – this results in a 5 mm-diameter disc corresponding to the macula

Importantly, eye movements can result in the displacement of the optic structures of several millimetres. An eye fixation protocol is therefore recommended to maximize the avoidance of the macula (for example, the protocol described by Buchgeister et al. [23]).

5. *Optic tract ("OpticTract_R" and "OpticTract_L")*

Each optic tract should be contoured separately. Co-registration with T1-weighted MRI is required for delineation. The optic tract extends from the postero-lateral angle of the optic chiasm anteriorly to the lateral geniculate body posteriorly [18]. It appears linear, hyperintense, and runs lateral to the hypothalamus and medial to the anterior perforated substance. The optic tract visibility is limited beyond the first 10–15 mm from the junction with the optic chiasm. Posteriorly, the contour extends at most until the thalamus but should be stopped when the optic tract is no longer clearly visible.

6. *Fornix ("Fornix_R" and "Fornix_L")*

The fornix (Figs. 1–3) constitutes the main output tract of the hippocampus and is thereby essential to memory consolidation [24].

Co-registration with T1-weighted MRI is required for delineation. The fornix is a C-shaped structure, formed of two symmetrical arch-like bundles of white matter, connecting the hippocampi inferoposteriorly to the mammillary bodies anteriorly. After leaving the hippocampi, these two bundles run initially medial to the temporal horn of the lateral ventricle. Then, they arch anterosuperiorly underneath the corpus callosum. They unite under the septum pellucidum. They finally diverge anteriorly, curving behind the anterior commissure and in front of the interventricular foramen (foramen of Monro). The contour stops at the cranial border of the mammillary bodies [18,19].

7. *Periventricular space ("PVS")*

Recent data suggest that the region bordering the ventricular system is more at risk of developing late radiation-induced contrast-enhancing lesions on MRI after radiotherapy. This is possibly due to the lower vascular supply in these areas as well as to variability in relative biological effectiveness (RBE) when using particle therapy [9-12,25]. In addition, the innermost region of the PVS, known as *subventricular zone*, constitutes a major neural stem cells niche and is associated with gliomagenesis [26,27].

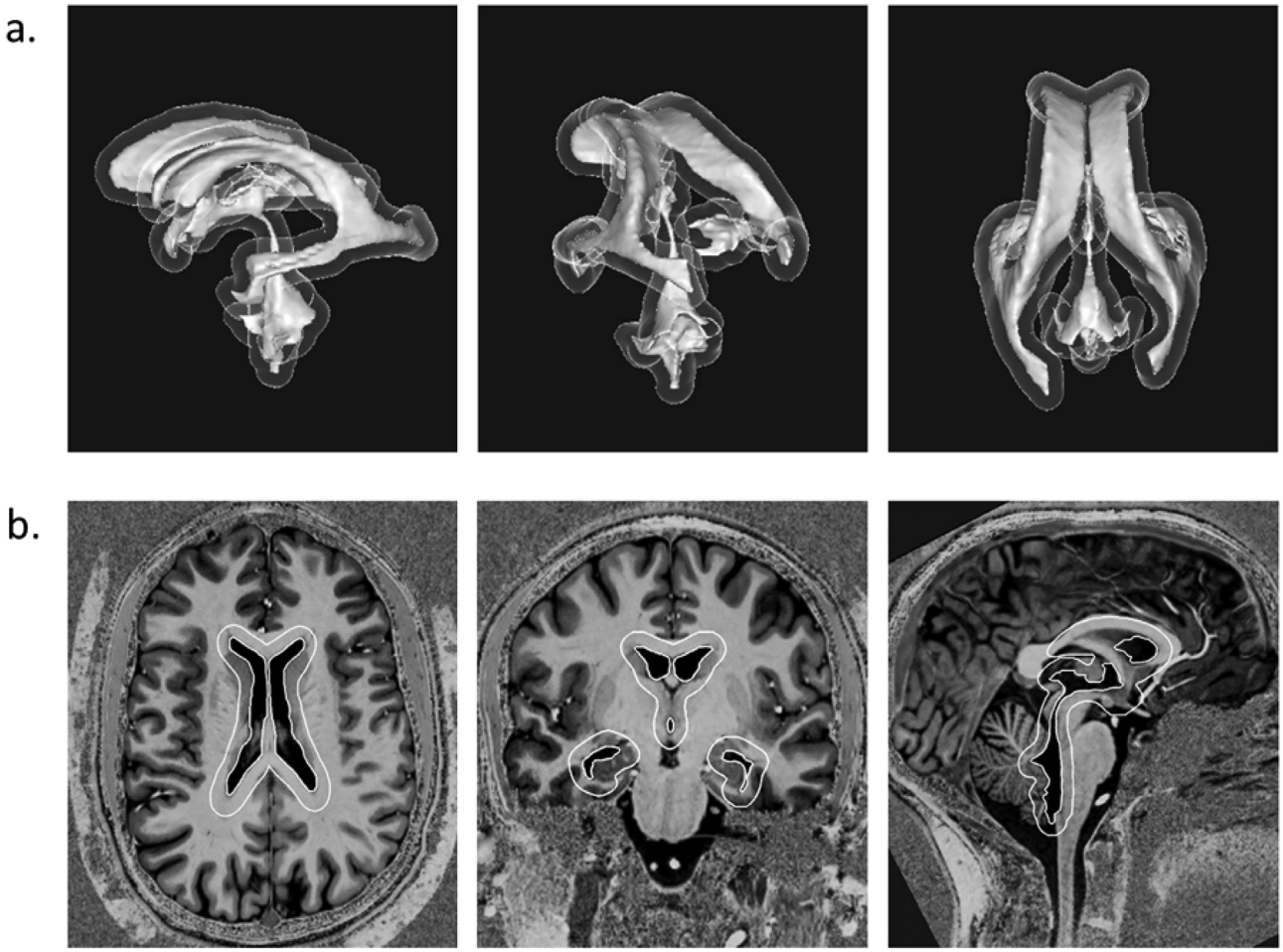

Fig. 5. Visualisation of the periventricular space (PVS) which is delineated as a 5 mm rim around the ventricular system (a) in 3D (PVS: semi-transparent white; ventricular system: white); (b) on a 7 T MRI (MP2RAGE) scan (from left to right: axial, coronal, and sagittal planes).

Co-registration with T1-weighted MRI is recommended for delineation. The PVS can be automatically delineated as the 5 mm rind of the ventricular system, which consists of the four ventricles and their connections (Fig. 5):

- The two lateral ventricles, including their different parts: frontal horn, central parietal part, occipital horn, and temporal horn
- The third ventricle, including the supraoptic recess, the infundibular recess, and the suprapineal recess
- The fourth ventricle
- The two Foramina of Monro, the Sylvian aqueduct, and the two foramina of Luschka

The configuration and width of the ventricular system can vary from one patient to another and some parts can be difficult to delineate (e.g. due to ventricular collapse). Co-registration with T2-weighted MRI can therefore be helpful.

8. *Orbitofrontal cortex ("Orbitofrontal_R" and "Orbitofrontal_L")*

The orbitofrontal cortex (OFC) (Figs. 1 and 2) is the region of the cortex located at the ventral side of the frontal lobe. It plays a key-role in memory, emotional functioning and cognition, in particular reward-based decision making [28]. The following delineation method is largely based on the procedure described by Crespo-Facorro et al. [29].

Co-registration with T1-weighted MRI is required for delineation. The OFC is easier to identify in the coronal plane, halfway through the frontal lobe (3–4 cm from the frontal pole of the brain). At this level, the orbitofrontal cortex runs between the olfactory sulcus medially, and the lateral orbital sulcus laterally. Moving anteriorly, on one hand, the medial border of the OFC follows the olfactory sulcus (thereby excluding the gyrus rectus) until it disappears, then the OFC reaches the midline. On the other hand, the lateral border of the OFC follows the lateral orbital sulcus until it disappears, then the OFC follows an imaginary horizontal line located at the same level, until it reaches the frontal pole of the brain. Moving posteriorly, the medial border of the OFC follows the olfactory sulcus as well, while the lateral border progressively switches from the lateral orbital sulcus to the circular sulcus of the insula.

9. *Corpus callosum ("CorpusCallosum")*

The corpus callosum (Figs. 2 and 3) is a large bundle of white fibres connecting the two hemispheres. Radiation-induced injuries in this region were recently shown to be associated with attention and processing speed decline [30,31].

Co-registration with T1-weighted MRI is recommended for delineation. The corpus callosum is best identified on the sagittal plane where it appears as a C-shaped structure. It is approximately 10 cm long and 5–10 mm thick. Superiorly, it is bordered by the

interhemispheric fissure / falx cerebri, and by the cingulum. Inferiorly, it is bounded by the septum pellucidum and fornix (medially), and by the lateral ventricles (laterally). Anteriorly, the corpus callosum curves in front of the septum pellucidum and connects with the lamina terminalis. Posteriorly, it ends superior to the ampulla of Galen. The lateral borders were artificially set at the lateral border of the lateral ventricles.

10. *Pineal gland ("Glnd_pineal")*

The pineal gland (Figs. 1 and 2) is a small endocrine gland measuring approximately 8 mm in diameter and notably involved in the regulation of the sleep-wake cycle.

Co-registration with T1-weighted MRI is recommended for delineation. The pineal gland is located on the midline, in the quadrigeminal cistern. It is located posteriorly to the third ventricle, inferiorly to the splenium of the corpus callosum, and anteriorly to the ampulla of Galen. In adult patients, the pineal gland frequently shows cysts or calcifications (easily seen on CT imaging) [18].

The updated atlas, including all aforementioned OARs delineated on CT and MR (3 T and 7 T), as well as a 3D animation are freely available on www.cancerdata.org [13].

Discussion

We present here an update of the EPTN consensus-based atlas for CT- and MR-based contouring in neuro-oncology which was initially published in 2018 [1,2]. In the present update, ten new OARs were added, i.e. amygdala, caudate nucleus, corpus callosum, fornix, macula, optic tract, orbitofrontal cortex, periventricular space, pineal gland, and thalamus.

The aim of this atlas is to reduce OARs delineation variability between RTOs/RTTs and between radiotherapy centres, both in photon and in particle therapy. Similarly, guidelines aiming at harmonising target volume delineation in the field of neuro-oncology have been recently published for glioblastoma [32] and skull base tumours [3]. Importantly, uniform delineation is a prerequisite for the implementation of large-scale clinical trials in the field of neuro-oncology, as well as for the accumulation of uniform toxicity data. This, in turn, will allow to improve existing normal tissue complication probability (NTCP) models and to establish new ones. In particular, there is currently a lack of appropriate NTCP models in relation with cognitive toxicity. Such models can in particular be used to select the patients who are expected to benefit from particle therapy in comparison with photon therapy (*i.e.*, the model-based approach used in The Netherlands [33]).

The OARs which were added in the present update were chosen based on their supposed clinical relevance. First, several of them could be associated with cognitive toxicity (*i.e.*, amygdala, caudate nucleus, corpus callosum, fornix, orbitofrontal cortex, pineal gland, and thalamus). Indeed, recent data suggests that radiation to the thalamus may lead to executive function and processing speed decline [34]. For the thalamus and the amygdala, a dose-dependent volume loss after radiotherapy was also observed [35]. Moreover, injuries to the corpus callosum were recently shown to be associated with attention/processing speed decline after radiotherapy [30,31]. Second, the macula and the optics tracts were added in order to allow for studying their role with regards to visual toxicity [36]. Third, the periventricular space was added as a result of accumulating data pointing to the development of radiation-induced lesions in this region after particle therapy [9-12]. Importantly, most of these OARs currently lack dose-constraints. Further work is therefore needed to precisely establish their clinical relevance and radiation tolerance. We suggest including these new OARs in future research projects, in particular those related to cognitive toxicity, in order to complement the currently available dose constraints in neuro-oncology [37].

Manual delineation is a time-consuming activity, which can be an obstacle for the clinician when it comes to contouring new OARs. In this context, artificial intelligence offers a promising route for the implementation of the delineation of more OARs on a large scale. A semi-automated contouring strategy for the OARs of the head and neck region using deep-learning was for example recently shown to lead to a 33% reduction of the contouring time [38]. In order to achieve this, the algorithms are trained using scans of different patients where the OARs are already contoured (training set). The present atlas can serve as a basis for generating homogeneous training sets, which can later be used to feed automatic contouring algorithms.

The list of OARs included in the present atlas is likely to evolve over time as a result of newly available data, leading for example to the modification of already described OARs, or to the addition of new ones. OARs to be potentially included in future updates include vascular structures (e.g. internal carotid artery or circle of Willis) and cranial nerves [39].

Conclusion

Uniform delineation of potentially relevant neurological OARs facilitates the implementation of multicentre trials (ensuring comparability between centers) and the development of future NTCP models, with the aim of enabling the clinicians to more precisely predict side effects after brain irradiation. The present atlas provides the base for delineation of 25 OARs on CT and MRI scans, including T1 post-gadolinium and T2 FLAIR sequences. A 7 T MRI scan was added for illustration purposes since 7 T is not widely available in daily practice. The updated neuro-oncology contouring atlas is freely available online on www.cancerdata.org and will be updated when indicated [13].

Acknowledgements

DDP is supported by a grant from Fondation Saint-Luc, Belgium. NGB is supported by the National Institute for Health Research Cambridge Biomedical Research Centre.

The authors sincerely thank: Lene Haldbo-Classen, MD PhD, Department of Radiotherapy, Aarhus University Hospital, for sharing her expertise in delineating the frontal lobe, Roel Germ Wanders, technician Maastro, for his help with processing the image data, and Noel Bauer, MD PhD, Department of Ophthalmology, Maastricht University Medical Centre+, for his help delineating the reconstructed fovea and macula.

Disclosure of Conflicts of Interest

The 7 Tesla MRI was supported by the Brains Unlimited Pioneer Fund of the Limburg University Fund/SWOL (S.2013.1.011).

Ethical publication statement

We confirm that we have read the journal's position on issues involved in ethical publication and affirm that this report is consistent with those guidelines. The work described has been carried out in accordance with The Code of Ethics of the World Medical Association (Declaration of Helsinki) for experiments involving humans. The manuscript is in line with the Recommendations for the Conduct, Reporting, Editing and Publication of Scholarly Work in Medical Journals and aim for the inclusion of representative human populations (sex, age and ethnicity) as per those recom-

mendations. The terms sex and gender are used correctly. The privacy rights of human subjects were always observed.

References

[1] Eekers DB, In 't Ven L, Roelofs E, Postma A, Troost EGC (2017) EPTN International Neurological Contouring Atlas. CancerData. doi:10.17195/candat.2017.08.1

[2] Eekers DB, In 't Ven L, Roelofs E, Postma A, Alapetite C, Burnet NG, et al. The EPTN consensus-based atlas for CT- and MR-based contouring in neuro-oncology. Radiother Oncol 2018;128:37–43. https://doi.org/10.1016/j.radonc.2017.12.013.

[3] Combs SE, Baumert BG, Bendszus M, Bozzao A, Brada M, Fariselli L, et al. ESTRO ACROP guideline for target volume delineation of skull base tumors. Radiother Oncol 2021;156:80–94. https://doi.org/10.1016/j.radonc.2020.11.014.

[4] Yang H, Mir R, Díez P, Tsang Y, Conibear J, Simões R, et al. Provision of Organ at Risk Contouring Guidance in UK Radiotherapy Clinical Trials. Clin Oncol (R Coll Radiol) 2020;32:e60–6. https://doi.org/10.1016/j.clon.2019.09.054.

[5] Pötter R, Balosso J, Baumann M, Bert C, Davies J, Enghardt W, et al. Union of light ion therapy centers in Europe (ULICE EC FP7) – Objectives and achievements of joint research activities. Radiother Oncol 2018;128:83–100. https://doi.org/10.1016/j.radonc.2018.04.027.

[6] Grau C, Durante M, Georg D, Langendijk JA, Weber DC. Particle therapy in Europe. Mol Oncol 2020;14:1492–9. https://doi.org/10.1002/1878-0261.12677.

[7] Jacob J, Clausse E, Benadjaoud MA, Jenny C, Ribeiro M, Feuvret L, et al. Dose distribution of the brain tissue associated with cognitive functions in high-grade glioma patients. Cancer Radiother 2020;24:1–10. https://doi.org/10.1016/j.canrad.2019.08.009.

[8] Florijn MA, Sharfo AWM, Wiggenraad RGJ, van Santvoort JPC, Petoukhova AL, Hoogeman MS, et al. Lower doses to hippocampi and other brain structures for skull-base meningiomas with intensity modulated proton therapy compared to photon therapy. Radiother Oncol 2020;142:147–53. https://doi.org/10.1016/j.radonc.2019.08.019.

[9] Harrabi S, Gudden C, Adeberg S, Bougatf N, Haberer T, Rieken S, et al. Radiation necrosis after proton beam therapy - when and where does it happen? [abstract]. Radiother Oncol 2017;123:S271. https://doi.org/10.1016/S0167-8140(17)30954-4.

[10] Harrabi S, Bauer J, Bahn E, Adeberg S, Haberer T, Alber M, et al. Radiation-Induced Brain Injury after Proton Radiotherapy Is Linked to Increased Distal Edge Linear Energy Transfer (LET) and Anatomically Variable Radiation Sensitivity. International journal of radiation oncology, biology. physics 2019;105:E99. https://doi.org/10.1016/j.ijrobp.2019.06.2289.

[11] Bahn E, Bauer J, Harrabi S, Herfarth K, Debus J, Alber M. Late contrast enhancing brain lesions in proton-treated patients with low-grade glioma: clinical evidence for increased periventricular sensitivity and variable RBE. Int J Radiat Oncol Biol Phys 2020;107:571–8. https://doi.org/10.1016/j.ijrobp.2020.03.013.

[12] Eulitz J, Troost EGC, Raschke F, Schulz E, Lutz B, Dutz A, et al. Predicting late magnetic resonance image changes in glioma patients after proton therapy. Acta Oncol 2019;58(10):1536–9. https://doi.org/10.1080/0284186X.2019.1631477.

[13] Eekers D, Di Perri D, Roelofs E, Postma A, Troost EG. EPTN International Neurological Contouring Atlas - 2021 Update. CancerData, 2021. doi:10.17195/candat.2021.02.1

[14] Brouwer CL, Steenbakkers RJHM, Bourhis J, Budach W, Grau C, Grégoire V, et al. CT-based delineation of organs at risk in the head and neck region: DAHANCA, EORTC, GORTEC, HKNPCSG, NCIC CTG, NCRI, NRG Oncology and TROG consensus guidelines. Radiother Oncol 2015;117:83–90. https://doi.org/10.1016/j.radonc.2015.07.041.

[15] Compter I, Peerlings J, Eekers DB, Postma AA, Ivanov D, Wiggins CJ, et al. Technical feasibility of integrating 7 T anatomical MRI in image-guided radiotherapy of glioblastoma: a preparatory study. MAGMA 2016;29:591–603. https://doi.org/10.1007/s10334-016-0534-7.

[16] Santanam L, Hurkmans C, Mutic S, van Vliet-Vroegindeweij C, Brame S, Straube W, et al. Standardizing naming conventions in radiation oncology. Int J Radiat Oncol Biol Phys 2012;83:1344–9. https://doi.org/10.1016/j.ijrobp.2011.09.054.

[17] Janak PH, Tye KM. From circuits to behaviour in the amygdala. Nature 2015;517:284–92. https://doi.org/10.1038/nature14188.

[18] Osborne AG. Imaging anatomy: brain and spine. Philadelphia: Elsevier; 2020.

[19] Sorce C, Chalaszczyk A, Rossi F, Ferella L, Grimaldi G, Splendiani A, et al. Recommendation for the contouring of limbic system in patients receiving radiation treatment: A pictorial review for the everyday practice and education. Crit Rev Oncol Hematol 2021;159:103229. https://doi.org/10.1016/j.critrevonc.2021.103229.

[20] Graff-Radford J, Williams L, Jones DT, Benarroch EE. Caudate nucleus as a component of networks controlling behavior. Neurology 2017;89:2192–7. https://doi.org/10.1212/WNL.0000000000004680.

[21] Wolff M, Vann SD. The cognitive thalamus as a gateway to mental representations. J Neurosci 2019;39:3–14. https://doi.org/10.1523/JNEUROSCI.0479-18.2018.

[22] American Academy of Ophthalmology. Fundamentals and principles of ophthalmology. San Francisco: American Academy of Ophthalmology; 2019.

[23] Buchgeister M, Grisanti S, Susskind D, Bamberg M, Paulsen F. A new fixation aid for the radiotherapy of eye tumors. Med Phys 2007;34:4649–53. https://doi.org/10.1118/1.2804750.

[24] Fletcher E, Raman M, Huebner P, Liu A, Mungas D, Carmichael O, et al. Loss of fornix white matter volume as a predictor of cognitive impairment in cognitively normal elderly individuals. JAMA Neurol 2013;70:1389. https://doi.org/10.1001/jamaneurol.2013.3263.

[25] Mamlouk MD, Handwerker J, Ospina J, Hasso AN. Neuroimaging findings of the post-treatment effects of radiation and chemotherapy of malignant primary glial neoplasms. Neuroradiol J 2013;26:396–412. https://doi.org/10.1177/197140091302600405.

[26] Lee JH, Lee JE, Kahng JY, Kim SH, Park JS, Yoon SJ, et al. Human glioblastoma arises from subventricular zone cells with low-level driver mutations. Nature 2018;560:243–7. https://doi.org/10.1038/s41586-018-0389-3.

[27] Valiyaveettil D, Malik M, Akram KS, Ahmed SF, Joseph DM. Prospective study to assess the survival outcomes of planned irradiation of ipsilateral subventricular and periventricular zones in glioblastoma. Ecancermedicalscience 2020;14:1021. https://doi.org/10.3332/ecancer.2020.1021.

[28] Rolls ET, Cheng W, Feng J (2020) The orbitofrontal cortex: reward, emotion and depression. Brain Commun 2:fcaa196. doi:10.1093/braincomms/fcaa196.

[29] Crespo-Facorro B, Kim J-J, Andreasen NC, O'Leary DS, Wiser AK, Bailey JM, et al. Human frontal cortex: an MRI-based parcellation method. Neuroimage 1999;10(5):500–19. https://doi.org/10.1006/nimg.1999.0489.

[30] Huynh-Le M-P, Tibbs MD, Karunamuni R, Salans M, Tringale KR, Yip A, et al. Microstructural injury to corpus callosum and intra-hemispheric white matter tracts correlate with attention and processing speed decline after brain radiation. Int J Radiat Oncol Biol Phys 2021;110:337–47. https://doi.org/10.1016/j.ijrobp.2020.12.046.

[31] Redmond KJ, Hildreth M, Sair HI, Terezakis S, McNutt T, Kleinberg L, et al. Association of neuronal injury in the genu and body of corpus callosum after cranial irradiation in children with impaired cognitive control: a prospective study. Int J Radiat Oncol Biol Phys 2018;101:1234–42. https://doi.org/10.1016/j.ijrobp.2018.04.037.

[32] Niyazi M, Brada M, Chalmers AJ, Combs SE, Erridge SC, Fiorentino A, et al. ESTRO-ACROP guideline "target delineation of glioblastomas. Radiother Oncol 2016;118:35–42. https://doi.org/10.1016/j.radonc.2015.12.003.

[33] Widder J, van der Schaaf A, Lambin P, Marijnen CAM, Pignol J-P, Rasch CR, et al. The quest for evidence for proton therapy: model-based approach and precision medicine. Int J Radiat Oncol Biol Phys 2016;95:30–6. https://doi.org/10.1016/j.ijrobp.2015.10.004.

[34] Haldbo-Classen L, Amidi A, Lukacova S, Wu LM, Oettingen GV, Lassen-Ramshad Y, et al. Cognitive impairment following radiation to hippocampus and other brain structures in adults with primary brain tumours. Radiother Oncol 2020;148:1–7. https://doi.org/10.1016/j.radonc.2020.03.023.

[35] Nagtegaal SHJ, David S, Philippens MEP, Snijders TJ, Leemans A, Verhoeff JJC. Dose-dependent volume loss in subcortical deep grey matter structures after cranial radiotherapy. Clin Transl Radiat Oncol 2021;26:35–41. https://doi.org/10.1016/j.ctro.2020.11.005.

[36] Fallico M, Chronopoulos A, Schutz JS, Reibaldi M. Treatment of radiation maculopathy and radiation-induced macular edema: A systematic review. Surv Ophthalmol 2021;66:441–60. https://doi.org/10.1016/j.survophthal.2020.08.007.

[37] Lambrecht M, Eekers DBP, Alapetite C, Burnet NG, Calugaru V, Coremans IEM, et al. Radiation dose constraints for organs at risk in neuro-oncology; the European Particle Therapy Network consensus. Radiother Oncol 2018;128:26–36. https://doi.org/10.1016/j.radonc.2018.05.001.

[38] van der Veen J, Willems S, Deschuymer S, Robben D, Crijns W, Maes F, et al. Benefits of deep learning for delineation of organs at risk in head and neck cancer. Radiother Oncol 2019;138:68–74. https://doi.org/10.1016/j.radonc.2019.05.010.

[39] Biau J, Dunet V, Lapeyre M, Simon C, Ozsahin M, Grégoire V, et al. Practical clinical guidelines for contouring the trigeminal nerve (V) and its branches in head and neck cancers. Radiother Oncol 2019;131:192–201. https://doi.org/10.1016/j.radonc.2018.08.020.